Simultaneous enhancement in open circuit voltage and short circuit current of hybrid organic-inorganic photovoltaics by inorganic interfacial modification

Yvonne J. Hofstetter,[ab] Paul E. Hopkinson,[ab] Artem A. Bakulin[c] and Yana Vaynzof[ab]

One of the key advantages of metal oxide/polymer organic-inorganic hybrid photovoltaic devices is the possibility to control the photo-induced charge separation efficiency by interfacial modification. While a large variety of organic modifiers have been investigated, inorganic modification layers remain largely unexplored. Here, we investigate the model poly(3-hexathiophene)/ZnO system and show that by introducing a caesium carbonate interlayer, a simultaneous increase in all photovoltaic performance parameters can be achieved. While improved energy level alignment results in a significant increase in the open circuit voltage, the suppression of interfacial bound charge pairs formation causes a reduction in interfacial recombination losses and an increase in short circuit current. The overall power conversion efficiency is enhanced twelve fold, demonstrating the significant potential of inorganic modifiers for improving the performance of hybrid photovoltaic devices.

Introduction

Hybrid photovoltaic devices combine favorable features of organic and inorganic semiconductors, functioning as the electron donor and acceptor, respectively. Such devices can profit from the strong absorption of the organic molecule, for example the polymer poly(3-hexathiophene), and the advantageous charge transport properties of the inorganic, which can include metal oxides like ZnO.[1] Additionally, hybrid photovoltaics offers the possibility for structural control that is difficult to achieve in all-organic PV, while having processing routes that are comparable in cost and complexity to all-organic devices. Despite these promising properties, power conversion efficiencies of hybrid PV devices remain relatively low.[2-7]

In addition to the advantages of combining the beneficial properties of both organic and inorganic materials, hybrid devices offer the possibility to introduce a modification layer between the donor and acceptor materials. This is significantly more difficult to achieve in organic-organic photovoltaic systems.[8,9] A large variety of organic modifiers have been investigated in literature. McGehee and co-workers investigated a variety of molecular interface modifiers with different dipole moments and found that modifiers that resulted in an increase in open circuit voltage (V_{oc}) caused a decrease in short-circuit current (J_{sc}) and vice versa.[10] Yoshikawa et al. investigated a variety of molecular dyes as modifiers and found that some dyes may result in a simultaneous increase in V_{oc} and J_{sc}, while others do not.[11] A self-assembled monolayer of phenyl-C61-butyric acid (PCBA) has been thoroughly investigated by us and others [2,3,4,12,13] and has been shown to significantly improve the performance of hybrid P3HT/ZnO PV devices by increasing J_{sc} as a result of decreased interfacial recombination and improved exciton dissociation.[2,3]

An increase in the V_{oc} by an organic modification of a hybrid organic-inorganic PV device is typically achieved by altering the energy level alignment at the polymer/oxide interface using either the inherent dipole of the organic molecule [10] or ground state charge transfer across the hybrid interface.[3] A variety of studies have demonstrated the efficacy of this approach, for example Schlesinger et al. and Timpel et al. who were able to modulate the work function (WF) of ZnO over a wide range by adsorption of either a (sub-)monolayer of 2,3,5,6-tetrafluoro-7,7,8,8-tetracyanoquinodimethane (F_4TCNQ) or phosphonate-based SAMs.[14,15]

Contrary to organic modifiers, inorganic modification layers remain largely unexplored in hybrid photovoltaics. Plank et al. reported that MgO and ZrO_2 modification of ZnO nanowires materials improved the efficiency of dye-sensitized hybrid solar cells due to an enhanced charge carriers separation, demonstrating the potential of inorganic modification layers in improving the performance of hybrid photovoltaics.[16,17] Lee et al. applied a thin layer of TiO_x to sol-gel deposited ZnO in both planar and nanowire forms, and reported an increase in V_{oc} from ~0.1 V to 0.5 V.[18]

Cs_2CO_3 has been previously utilized as a modification layer in polymer light emitting diodes (PLEDs) and has been shown to reduce the injection barrier into the polymer.[19,20] It has also been used in all-organic photovoltaics based on poly(3-hexylthiophene):[6,6]-phenyl C61 butyric acid methyl ester (P3HT:PCBM) bulk heterojunction solar cells.[21] The layer can be easily deposited from solution and is just as suitable for modification of interfaces in hybrid photovoltaic devices. We investigate the effect of this modifier on the photovoltaic (PV) performance and demonstrate that an inorganic modifier can result in a significant enhancement in the efficiency of charge separation as well as improved energy level alignment at the hybrid interface. These effects result in a significant increase in both the V_{oc} and J_{sc} of the PV device, with an overall efficiency improvement surpassing that of any organic modifier used in the model bilayer ZnO/P3HT system. Additionally, the performance is superior to that of a bilayer P3HT/PCBM PV device and does not require the use of a fullerene derivative.[8] This should open new possibilities for improvement in hybrid photovoltaics and deepen the understanding of charge separation processes taking place at hybrid organic-inorganic interfaces.

Experimental

Chemicals and solution preparation

P3HT (Mw=78 kg/mol, PDI < 2.2, RR > 96%, chemical structure shown in Figure 1) was purchased from 1-Material. All other chemicals were purchased from Sigma-Aldrich. All materials were used without further purification.

The ZnO solution was prepared following the method of Kwon *et al.*[22] where 0.46 M zinc acetate dihydrate (99.999%) and 0.46M ethanolamine (99.5%) are dissolved in 2-methoxyethanol (anhydrous, 99.8%) while being stirred on a hot plate at 70 °C for approximately two hours.

For the interlayer deposition, a 5 mg/ml solution of Cs_2CO_3 (99.995%, chemical structure in Figure 1) in 2-ethoxyethanol (99%) was prepared. It was dissolved while being stirred on a hot plate at 70 °C for one hour.

In a nitrogen purged glovebox (O_2, H_2O < 1ppm), the P3HT was dissolved in chlorobenzene (10 mg/ml; anhydrous, 99.8%) on a hot plate at 70 °C for one to two hours. After dissolving, the solution was filtered and allowed to cool to room temperature before proceeding with device fabrication.

Device fabrication

Pre-patterned ITO coated glass substrates (PsiOTec Ltd, UK) were first sonicated in acetone, then in isopropanol for 5min each and then etched in oxygen plasma for 10 min. Immediately after plasma cleaning, the ZnO solution was spin coated at 2000 rpm for 45 s onto the ITO and annealed for 30 min at 200 °C in air. On top of the ZnO, the Cs_2CO_3 solution was spin coated for 45 s at 5000 rpm and annealed for 20 min at 155 °C in air. Next, the samples were transferred to the nitrogen glovebox where then the P3HT solution was spin coated for 45 s at 2000 rpm. Following the deposition of the P3HT, 7 nm of MoO_3 and 80 nm of Ag were thermally evaporated under high vacuum (<1x10^{-6} mbar). After the evaporation, the devices were annealed for 20 min at 155°C (in nitrogen). Finally, metal legs were added contacting the ITO and Ag, and the completed devices encapsulated using 2-component epoxy adhesive and cover glasses before removal from the glovebox for measurements in air. The final PV device structure is shown in Figure 1.
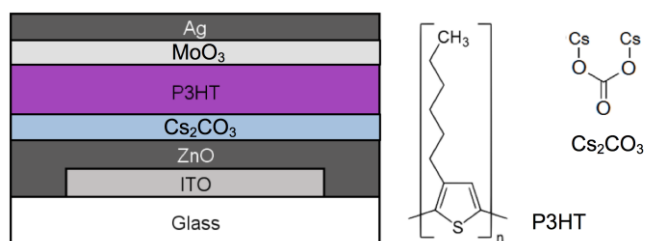

Figure 1: (left) Architecture of the inverted hybrid PV device investigated in this study; (right) Chemical structure of P3HT and Cs_2CO_3.

Experimental methods

UV-Vis. Films for UV-Vis characterization were prepared on glass in an identical fashion to those used in devices. The samples were analyzed with a Jasco V-670 UV-VIS-NIR spectrophotometer.

Atomic force microscopy (AFM): The atomic force microscope (Bruker MultiMode) was used in tapping mode in air with silicon tips (Nanosensors PPP-NCH) to study the surfaces of ZnO and Cs_2CO_3.

External quantum efficiency (EQE): EQE was measured with the monochromated light of a halogen lamp (range: 375nm to 700nm), calibrated with a NIST-traceable Si diode (Thorlabs).

J-V curves: A source-measure unit (Keithley 2450) was used to record current-voltage curves in the dark, and with the PV devices illuminated under AM1.5 conditions (ABET Sun 3000 class AAA solar simulator).

Transient photovoltage (TPV): A function generator (Agilent/Keysight 33510B) was used to pulse an inorganic LED (λ=525 nm, pulse length=250 µs), the light from which was focused onto the active area of the PV device. The resulting transient photovoltage in the device was measured across the 1 MΩ input impedance of an oscilloscope (Picoscope 5443A).

Pump-push photocurrent spectroscopy: The output of a regenerative 1 kHz Ti:Sapphire amplifier system (Spectra Physics Solstice, 800 nm, 100 fs pulse duration, 3 mJ per pulse) was split into two parts. One part was used to pump a broadband non-collinear optical amplifier to generate visible pump pulses (100 fs pulse duration, 2.3 eV photon energy). Another part was used to generate mid-IR push pulses by pumping an optical parametric amplifier (TOPAS, 150 fs pulse duration, 0.5 eV photon energy).

In the pump-push photocurrent experiments all devices were measured at short-circuit conditions. Pump pulses (in the order of 10 nJ) and ~1 µJ push pulses were focused onto a ~0.5 mm^2 spot on the device. The reference photocurrent induced in the studied device by the pump was detected at the laser repetition frequency of 1 kHz by a lock-in amplifier. The push beam was mechanically modulated at ~380 Hz, and its effect on the photocurrent was detected by a lock-in amplifier locked to the chopper frequency.

X-ray and ultraviolet photoemission spectroscopy (XPS and UPS): Thin films of P3HT (4 mg/ml P3HT solution was spin coated at 3000 rpm) were deposited on ZnO and Cs_2CO_3/ZnO and post-annealed at 155 °C. The samples were then transferred to the ultrahigh vacuum chamber (ESCALAB 250Xi) for XPS/UPS measurements. The measurements were carried out using a XR6 monochromated Al Kα source (hv = 1486.6 eV) and pass energy of 20 eV. UPS measurements were performed using a He discharge lamp (hv = 21.2 eV) and pass energy of 2 eV.

Results and discussion

Optical properties, composition and morphology

To characterize the properties of the inorganic modification layer, we have investigated bare and modified ZnO films. Absorption measurements (Figure 2) show that the UV absorption features of the ZnO (peak at 295 nm) do not overlap with those of P3HT, which absorbs in the visible. The P3HT spectrum exhibits both the main peak at 520 nm and two shoulders at 550 nm and 600 nm, as has been previously observed for crystalline P3HT.[23] The long-wavelength cutoff in the P3HT and ZnO absorption spectra indicate (optical) bandgaps of 1.9 eV and 3.3 eV, respectively.

In comparison to the ZnO and P3HT, the Cs_2CO_3 interlayer introduces very little absorption, mainly in the UV (absorption peak at 365 nm). Hence, there are no significant differences in the active

layer absorption properties between the unmodified and Cs_2CO_3 modified device.
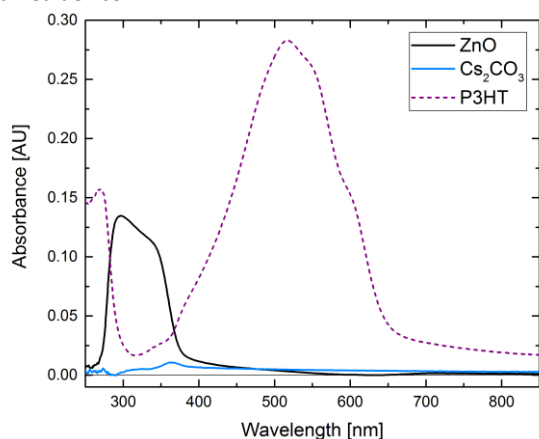

Figure 2: UV-Vis absorbance spectra of each layer in the solar cell: ZnO, Cs_2CO_3, and P3HT.

XPS measurements were carried out to investigate the composition of the bare and modified ZnO layers. Figure 3a-d shows the survey spectra collected on ZnO and Cs_2CO_3/ZnO, as well as the Zn2p, O1s and Cs3d regions. The binding energies of the Zn2p doublet are 1022.8 eV and 1045.8 eV, in agreement with previous measurements.[3] The O1s signal shows two peaks at different
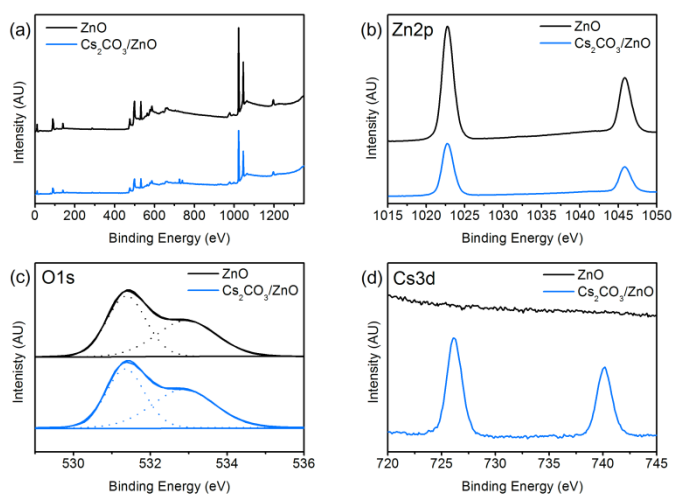

Figure 3: XPS spectra of a ZnO and a Cs_2CO_3/ZnO sample. Shown are (a) the whole spectra, and closer ranges of relevant peaks: (b) Zn 2p , (c) O 1s, and (d) Cs 3d.

binding energies corresponding to two different species of O-atoms: the low binding energy peak is assigned to O-Zn atoms in ZnO and the high binding energy peak is related to oxygen in hydroxyl groups (OH). The Cs_2CO_3/ZnO sample shows a Cs3d doublet, in agreement with previous measurements.[19] In addition to compositional characterization, XPS was used to determine the thickness of the Cs_2CO_3 interlayer. Because of the overlying Cs_2CO_3 layer, the Zn2p signal is attenuated. This attenuation makes it possible to estimate the thickness of the Cs_2CO_3 which we find to be ~1-2 nm.
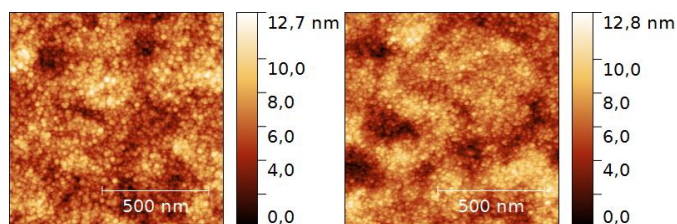

Figure 4: Representative AFM micrograph of the ZnO surface (left) and the Cs_2CO_3 surface (right), scanned area: $1\mu m^2$.

Table 1: Surface roughness (R_{RMS}) and surface area of the AFM micrographs in Figure 4.

	R_{RMS} [nm]	Surface area [μm^2]
ZnO	1.74	1.02
ZnO/Cs_2CO_3	1.76	1.02

Additionally, the surface of the ZnO and Cs_2CO_3/ZnO was investigated using atomic force microscopy (AFM). Figure 4 shows a representative 1 μm^2 AFM micrograph of each of the two samples. We observe no significant changes in the height profile and structure upon Cs_2CO_3 modification, indicating that Cs_2CO_3 forms a conformal coating of the underlying ZnO layer. Cs_2CO_3 layers exposed to chlorobenzene (the P3HT solvent) show no difference to unexposed layers (Figure S3 and Table S2). From the AFM measurements we determined the mean squared roughness (R_{RMS}) and the surface area. The R_{RMS} values for both ZnO and Cs_2CO_3/ZnO are approximately the same (1.74 nm and 1.76 nm, respectively), and the surface areas measures 1.02 μm^2 for both samples (see Table 1). Overall, both surfaces are very smooth with only a slight enhancement compared to the scanned area of 1 μm^2. These results are reproducible on a larger scale (see SI Figure S1).

Photovoltaic Properties

The photovoltaic performance of the unmodified and Cs_2CO_3 modified devices was characterized by external quantum efficiency (EQE) measurements and J-V characteristics measured under AM1.5 conditions. The performance of the best devices is shown in Figure 5a and 5b, while Table S3 summarizes the mean and standard deviation of the photovoltaic parameters of devices across several batches. As can be seen in Figure 5a, the unmodified device exhibits a peak EQE of about 6% at ~500 nm. This value is nearly doubled for the modified device, reaching 10% EQE. As expected, the general shape of the spectrum remains the same and resembles the P3HT absorption spectrum (Figure 2).

The current voltage curves measured under AM1.5 conditions (Figure 5b) show a significant improvement in the performance of the Cs_2CO_3 modified device. The measurements show that the open-circuit voltage (V_{oc}) is almost quadrupled, the short-circuit current (J_{sc}) is doubled (as expected from the EQE measurements) and the fill factor (FF) is increased by 40%. These improvements result in the overall power conversion efficiency (PCE) drastically increasing from 0.04% to 0.48%. The V_{oc}, J_{cs}, FF and PCE parameters are summarized in Table 2.
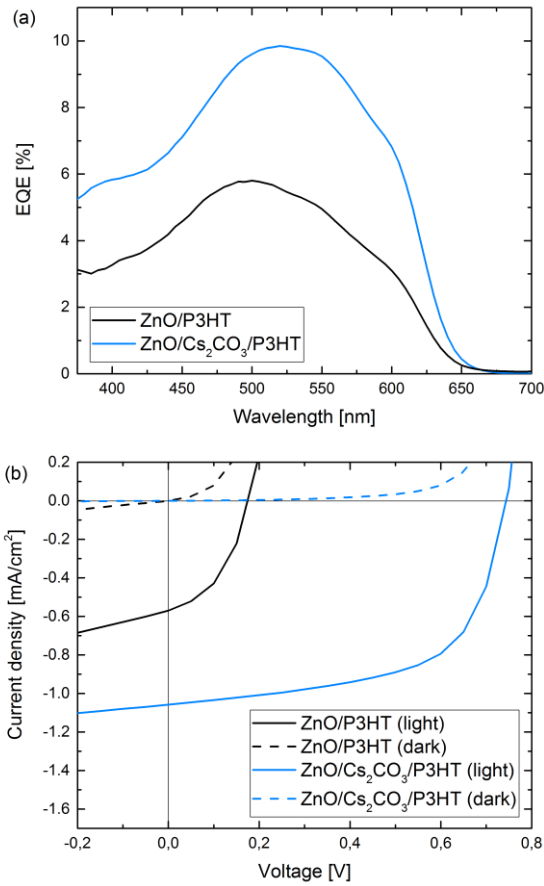
Figure 5: Photovoltaic characterization by (a) EQE measurements and (b) I-V curves of the best pixels on PV devices with and withoutF Cs₂CO₃ interlayer.

Table 2: Peak EQE and J-V parameters of the curves in Figure 5.

	EQE [%]	V_{oc} [V]	J_{sc} [mA/cm²]	FF [%]	PCE [%]
ZnO/P3HT	5.8	0.17	-0.57	43.2	0.04
ZnO/Cs₂CO₃/P3HT	9.8	0.74	-1.06	60.5	0.48

Investigating the improvement in open circuit voltage and short circuit current

To investigate the origin of the improvement in V_{oc}, UPS measurements were performed to study possible changes in energetics due to the Cs₂CO₃ interlayer. From the secondary photoemission onsets shown in Figure 6a and c, the work functions (WF) of the various layers were determined. In the unmodified case, the WF is measured to be 3.6 eV for both ZnO and P3HT/ZnO. This indicates that there is a vacuum level alignment at the hybrid interface in the case of the unmodified device. Upon modification with Cs₂CO₃ the WF of ZnO is lowered to 3.1 eV, resulting in the WF of P3HT/Cs₂CO₃/ZnO also decreasing to 3.1 eV.

The low binding energy edge in Figure 6b and d allows us to determine the position of the valence band (VB) edge of ZnO or Cs₂CO₃/ZnO and the position of the highest unoccupied molecular orbital (HOMO) of the P3HT on both surfaces with respect to the Fermi level.

The VB edge both of ZnO and Cs₂CO₃/ZnO is found to be 3.3 eV below the Fermi level, consistent with the absorption measurements shown previously. There is, however, a significant shift of the HOMO level of the P3HT with respect to the Fermi level in the polymer. In the unmodified case the P3HT HOMO is 0.9 eV below the Fermi level, while in the Cs₂CO₃ modified interface, it is measured to be 1.4 eV below the Fermi level.

The band gap energies of ZnO and P3HT were estimated from the UV-Vis spectra (Figure 2): 3.3 eV for ZnO and 1.9 eV for P3HT. Assuming that the optical gap is similar to the transport gap in these materials, we can estimate the positions of the conduction band (CB) of the ZnO and the lowest unoccupied molecular orbital (LUMO) of the P3HT in order to construct a complete representation of the energy level diagrams for both the unmodified and modified hybrid interfaces. These diagrams are shown in the bottom part of Figure 6.

The energetic difference between the HOMO of the P3HT and the CB of the ZnO corresponds to the maximum V_{oc} that could be obtained in a photovoltaic device. We observe an increase in $V_{oc,max}$ from 0.9 eV to 1.4 eV in the unmodified and Cs₂CO₃ modified interfaces, respectively. This increase is in an excellent agreement with the measured increase in device V_{oc}, with the unmodified device reaching a V_{oc} of 0.17 V whereas for the device with Cs₂CO₃ interlayer reaching $V_{oc} = 0.74$ V (Table 2). The beneficial effect of an increase in the photovoltaic bandgap ($V_{oc,max}$) on the device V_{oc} was observed previously for hybrid P3HT/ZnO devices in the case of Mg doping of the ZnO layer.[24,25] Therein, the authors report that Mg doping changes in the position of the CB of ZnO, resulting in an increase in $V_{oc,max}$ and thus, V_{oc}.
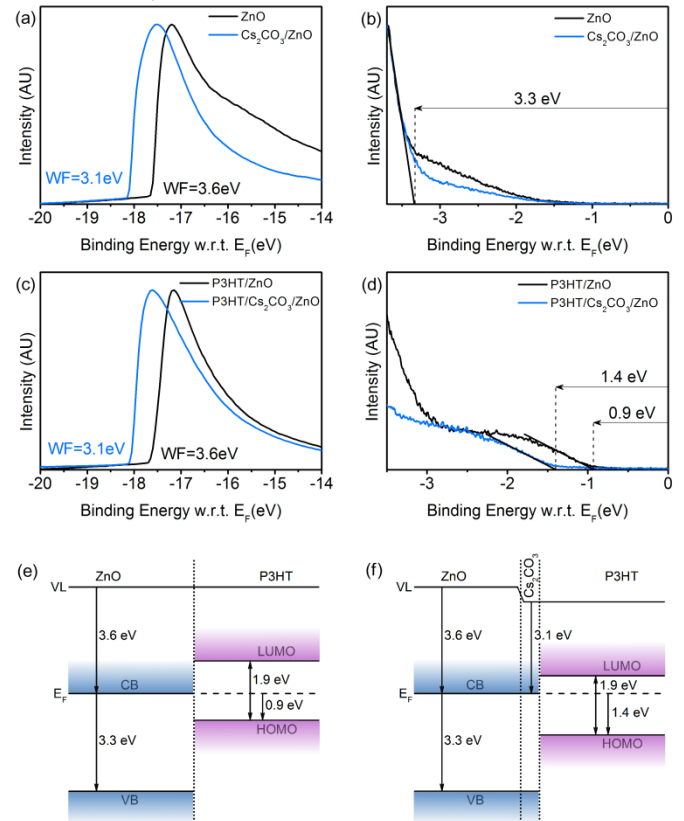

Figure 6: (a/b) UPS spectra of ZnO and Cs₂CO₃/ZnO, (c/d) UPS spectra of P3HT/ZnO and P3HT/Cs₂CO₃/ZnO, and the resulting energy level diagrams for the sample (e) without and (f) with Cs₂CO₃.

While the Cs_2CO_3 interlayer does not change the properties of the ZnO as Mg doping would, it decreases the work function of the modified surface, resulting in a similar increase in $V_{oc,max}$.

In addition to the significant enhancement in the V_{oc}, we observe a doubling of the J_{sc} upon introduction of the interlayer. While this increase could arise from an enhancement in the interfacial surface area between P3HT and the inorganic acceptor, previously presented AFM micrographs (Figure 4) show that this is not the case. Alternatively, the increase in current could be a result of increased crystallinity of P3HT,[26] however UV-Vis measurements on P3HT/ZnO and P3HT/Cs_2CO_3/ZnO (see SI Figure S2) show that no variation in the crystallinity of P3HT can be observed.
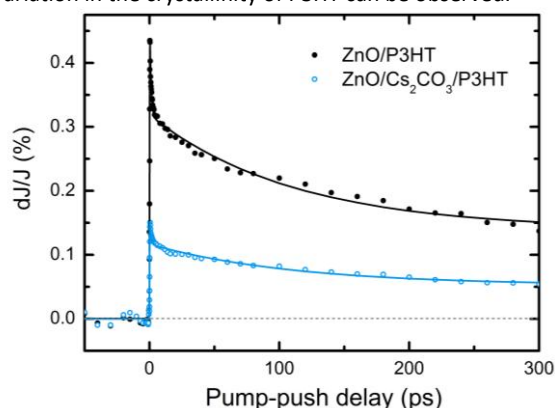

Figure 7: Pump-push photocurrent measurements of PV devices with and without Cs_2CO_3 interlayer

We have previously employed pump-push photocurrent (PPP) spectroscopy to characterize the efficiency of photo-induced charge carrier separation across the hybrid interface [2,4] and showed that bound charge pairs (BCP) form at this interface hindering the photovoltaic performance. The yield of BCPs can be significantly decreased by an organic modifier such as PCBA.[2] To check if the inorganic modifier has a similar beneficial effect on the yield of BCPs, PPP measurements were carried out on unmodified and Cs_2CO_3 modified devices. As can be seen in Figure 7, when the push pulse arrives after the pump pulse, we observe a prompt increase in dJ/J (proportional to the number of BCPs). This increase originates from the separation of BCPs prompted by the additional energy given by the push pulse. For the unmodified device, the signal is about three times stronger than for the Cs_2CO_3 modified device, indicating that charge separation at the modified hybrid interface is significantly more efficient than in the unmodified case. The reduction in the yield of BCPs is consistent with the enhancement in the short circuit current in the device. (Figure 5 and Table 2)
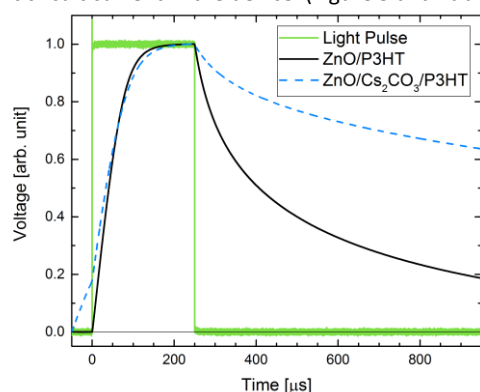

Figure 8: TPV characteristics of the best pixels on PV devices without and with Cs_2CO_3 interlayer upon excitation with a green LED.

An additional insight into the recombination losses in the devices can be obtained from transient photovoltage (TPV) measurements. The normalized signals of the devices and the light pulse (green LED) are shown in Figure 8. Comparing the TPV signals, one can see a slower decay (i.e. longer lifetime) of photogenerated carriers in the modified device. This increase in lifetime is consistent with a reduction of recombination losses and improved charge separation at the modified interface, in agreement with the PPP measurements.

We have previously proposed that the formation of BCPs across a hybrid interface is related to the localization of an electron in a surface trap state at the ZnO. This electron in turn Coulombically attracts the positive polaron on the adjacent P3HT polymer chain forming a bound charge pair. The inorganic modifier Cs_2CO_3 introduces a spatial separation between the trapped electron and the polymer, weakening the Coulombic attraction between the two charge carriers. While surface trap states in the inorganic modifier could act as localizing sites for electrons after charge transfer, our UPS measurements (Figure 6b) show that the density of sub bandgap states is significantly reduced upon inorganic modification. We believe that the combination of the reduction of surface trap states and increased spatial separation between charges is responsible for the increased efficiency of charge separation across the modified interface.

Conclusions

In this study we have demonstrated the tremendous potential of inorganic modifiers as interlayers in organic-inorganic photovoltaic devices. Using ultra-violet photoemission spectroscopy we have shown that advantageous energy level alignment increases the photovoltaic gap and as a result the open circuit voltage by ~0.5 V. In addition, the insertion of the inorganic interlayer lowers the yield of bound charge pairs forming at the hybrid interface resulting in a doubling of the short circuit current. The overall power conversion efficiency of the hybrid bilayer device, 0.48%, is the highest reported to date for any surface modifiers used for the P3HT/ZnO model system.

These promising results show that other inorganic modifiers, such as barium hydroxide or strontium hydroxide may be of great interest for hybrid photovoltaic modification and open a new route for the much needed improvement of the photovoltaic performance of these devices.

Acknowledgements

Notes and references

1   B. S. Ong, C. Li, Y. Li, Y Wu and R. Loutfy, *J. Am. Chem. Soc.*, 2007, **129**, 2750–2751.

2   Y. Vaynzof, A. A. Bakulin, S. Gélinas, and R. H. Friend, *Physical Review Letters*, 2012, **108**, 246605.

3   Y. Vaynzof, D. Kabra, L. Zhao, P. K. H. Ho, A. T.-S. Wee, and R. H. Friend, *Applied Physics Letters*, 2010, **97**, 033309.

4   O. Pachoumi, A. A. Bakulin, A. Sadhanala, H. Sirringhaus, R. H. Friend, and Y. Vaynzof, *Journal of Physical Chemistry C*, 2014, **118**, 18945-18950.

5   G. Mattioli, S. B. Djhil, M. I. Saba, G. Malloci, C. Melis, P. Alippi, F. Filippone, P. Giannozzi, A. K. Thakur, M. Gaceur, O. Margeat, A. K. Diallo, C. Videlot-Ackermann, J. Ackermann, A. A. Bonapasta and A. Mattoni, *Adv. Energy Mater.*, 2014, **4**, 1301694.

6   S. H. Eom, M. J. Baek, H. Park, L. Yan, S. Liu, W. You and S. H. Lee, *ACS Appl. Mater. Interfaces*, 2014, **6**, 803-810.

7   S. Wood, J. B. Franklin, P. N. Strvrinou, M. A. McLachlan and J.-S. Kim, *Appl. Phys. Lett.* 2013, **103**, 153304.

8   A. Tada, Y. Geng, Q. Wei, Qingshuo, K. Hashimoto, K. Tajima, *Nature Materials*, 2011, **10**, 450-455.

9   Z.-K. Tan, K. Johnson, Y. Vaynzof, A. A. Bakulin, L.-L. Chua, P. K. H. Ho, and R. H. Friend, *Advanced Materials*, 2013, **25**, 4131-4138.

10 C. Goh, S. R. Scully, and M. D. McGehee, *Journal of Applied Physics*, 2007, **101**, 114503.

11 P. Ruankham, L. Macaraig,. T. Sagawa, H. Nakazumi,. and S. Yoshikawa, *Journal of Physical Chemistry C*, 2011, **115**, 23809–23816.

12 K. Yao, L. Chen, Y. Chen, F. Li, and P. Wang, *Journal of Physical Chemistry C*, 2012, **116**, 3486–3491.

13 X. Wang and F. Chen, *Journal of Materials Science: Materials in Electronics*, 2015, **26**, 1125-1128.

14 R. Schlesinger, Y. Xu, O. T. Hofmann, S. Winkler, J. Frisch, J. Niederhausen, A. Vollmer, S. Blumstengel, F. Henneberger, P. Rinke, M. Scheffler, and N. Koch, *Physical Review B*, 2013, **87**, 155311.

15 M. Timpel, M. V. Nardi, S. Krause, G. Ligorio, C. Christodoulou, L. Pasquali, A. Giglia, J. Frisch, B. Wegner, P. Moras, and N. Koch, *Chemistry of Materials*, 2014, **26**, 5042-5050.

16 N. O. V. Plank, H. J. Snaith, C. Ducati, J. S. Bendall, L. Schmidt-Mende, and M. E. Welland, *Nanotechnology*, 2008, **19**, 465603.

17 N. O. V. Plank, I. Howard, A. Rao, M. W. B. Wilson, C. Ducati, R. S. Mane, J. S. Bendall, R. R. M. Louca, N. C. Greenham, H. Miura, R. H. Friend, H. J. Snaith, and M. E. Welland, *Journal of Physical Chemistry C*, 2009, **113**, 18515-18522.

18 Lee, Y.-J. et al. *IEEE J. Sel. Top. Quantum Electron.,* 2010, 16, 1587–1594.

19 Y. Vaynzof, D. Kabra, L. L. Chua, and R. H. Friend, *Applied Physics Letters*, 2011, **98**, 113306.

20 D. Kabra, L. P. Lu, M. H. Song, H. J. Snaith, and R. H. Friend, *Advanced Materials*, 2010, **22**, 3194–3198.

21 H.-H. Liao, L.-M. Chen, Z. Xu, G. Li and Y. Yang, *Appl. Phys. Lett.*, 2008, **92**, 173303.

22 S. Kwon, K.-G. Lim, M. Shim, H. C. Moon, J. Park, G. Jeon, J Shin, K. Cho, T.-W. Lee, and J. K. Kim, *J. Mater. Chem. A*, 2013, **1**, 11802.

23 Y. Kim, S. Cook, S. M. Tuladhar, S. A. Choulis, J. Nelson, J. R. Durrant, D. D. C. Bradley, M. Giles, I. McCulloch, C.-S. Ha and M. Ree, *Nat. Mater.* 2006, **5**, 197-203.

24 D. C. Olson, S. E. Shaheen, M. S. White, W. J. Mitchell, M. F. A. M. van Hest, R. T. Collins, and D. S. Ginley, *Adv. Funct. Mater.*, 2007, 17, 264–269.

25 R. L. Z. Hoye, D. Muñoz-Rojas, K. P. Musselman, Y. Vaynzof, and J. K. MacManus-Driscoll, *ACS Applied Materials and Interfaces*, 2015, **7**, 10684−10694.

26 J.-M. Chiu and Y. Tai, *ACS Applied Materials and Interfaces*, 2013, **5**, 6946–6950.